sustainability

MDPI

Article

Dynamics of Biochar-Silty Clay Interaction Using In-House Fabricated Cyclic Loading Apparatus: A Case Study of Coastal Clay and Novel Peach Biochar from the Qingdao Region of China

Junwei Liu [1], Suriya Prakash Ganesan [1,2], Xin Li [1], Ankit Garg [2,*], Aman Singhal [1,3], Karthik Datta Dosetti [1,3] and Haibao Feng [4]

1 Institute of Civil Engineering, Qingdao University of Technology, Shibei District, Qingdao 266033, China; liujunwei@qut.edu.cn (J.L.); suriyaganesan1075@gmail.com (S.P.G.); lixin950710@163.com (X.L.); as53@iitbbs.ac.in (A.S.); dkd11@iitbbs.ac.in (K.D.D.)
2 Department of Civil and Environmental Engineering, Guangdong Engineering Centre for Structure Safety and Health Monitoring, Shantou University, Jinping District, Shantou 515063, China
3 Department of Civil Engineering, Indian Institute of Technology Bhubaneswar, Bhubaneswar, Odisha 752050, India
4 State Key Laboratory of Hydraulic Engineering Simulation and Safety, Tianjin University, Nankai, Tianjin 300072, China; fenghaibao@ccccyhj.com
* Correspondence: ankit@stu.edu.cn

Received: 22 February 2020; Accepted: 23 March 2020; Published: 25 March 2020

check for updates

Abstract: Biochar has been recently investigated as an eco-friendly material in bio-engineered slopes/landfill covers. A majority of recent studies have focused on analyzing water retention behavior while very few have examined dynamic behavior (i.e., cyclic loading due to earthquake, wind, or wave) of biochar amended soil. As far as the authors are aware, there is no study on the dynamic behavior of biochar amended soils. Considering the above mentioned study as a major objective, field excavated soil was collected and mixed with in-house produced biochar from peach endocarps, at three amendment rates (5%, 10%, and 15%). The un-amended bare soil and biochar amended soil were imposed to a cyclic load in a self-designed apparatus and the corresponding stress-strain parameters were measured. Dynamic parameters such as shear modulus and damping ratio were computed and the results were compared between bare and biochar amended soil. Furthermore, the residual cyclic strength of each soil types were correlated with an estimated void ratio to understand the interrelation between dynamic loading responses and biochar amended soils. The major outcomes of this study show that the addition of biochar decreases the void ratio, thereby increasing the shear modulus and residual cyclic strength. However, the modulus and strength values attenuates after 15 cycles due to an increase in pore water pressure. In contrary, at higher amendment rates, Biochar Amended Soils (BAS) forms clay-carbon complex and decreases both shear modulus and residual cyclic strength.

Keywords: biochar amended soils; dynamic loading; shear modulus; residual cyclic strength; void ratio

1. Introduction

The conversion of organic bio-waste material into an energy has received significant attention as a sustainable alternative in various applications. The bio-derived resource materials serves as a solution for environmental management to scale down global threats such as Greenhouse gas emission, climate change, and waste management [1,2]. Further, the conversion of bioresource materials reduces the dependency of other resource materials and promotes the direction towards a bio-based economy [3,4]. In the purview of engineering, one such approach is biochar, obtained from one of the thermal conversions of biomass, termed as pyrolysis [5]. Primarily, the unique properties of biochar is considered an appropriate tool to impede climate change [6,7] and sequester carbon in the soil [8,9]. Later on, the properties on state of the art studies on Biochar Amended Soils (BAS) gained much recognition in several applications.

Over the past two decades, biochar has been utilized in diverse applications as a soil amendment because of its positive effects on soil water retention properties [10–12]. Several studies have substantiated that the addition of biochar in soil changes soil properties such as porosity, specific surface area, and surface properties, which in turn enhances the retention and mechanical parameters [13–16]. Resulting to this material favorableness, biochar amendment gained much recognition in agricultural and geo-environmental applications [17–19]. From an agricultural perspective, the addition of biochar in soil promotes crop yield and nutrient retention, which are widely established in several studies [20–22]. Concurrently, in geo-environmental applications, BAS were considered for its potential implementation on landfill liners and ground improvement in accordance with improvement on shear strength [23], better hydraulic performance [24], and mitigation of soil erosion [25]. Nevertheless the limitations of biochar such as leaching and toxicity were also added in the background of biochar studies [26,27].

Given the fact about the geo-environmental applications, most of the studies examined only the static loading behavior of BAS, with rare investigations on dynamic loading characteristics. While, in general, soil supporting offshore structures are subjected to varying dynamic loads such as wave, seismic, and wind loads and could experience extreme damage after several cycles [28,29]. Additionally, slopes like landfill liners could also be affected by seismic activity which leads the top layer to crack, allowing methane emission via the cracks [30]. The most common approach for mitigating such dynamic loading failures are either by the dynamic compaction of soils or amendment by adequate stabilizing materials such as cement or calcium rich materials [31]. This raises a question: Is biochar a suitable amendment material to alleviate these failures?

Recent studies elucidated that the biochar amendment in sandy soils increases the cyclic resistance and confirms that biochar could be used as a potential material for liquefaction mitigation [32,33]. The above mentioned studies defined that owing to biochar's material properties, their amendment on sandy soils might alter certain soil characteristics, which in turn improve the cyclic resistance. However, these studies failed to present clear-cut explanations and depicted few considerable hypothesis on void ratio and the porous nature of biochar. Additionally, the investigation was limited only to the sandy soils with lesser biochar amendment rates.

In this study, the mentioned research gaps were taken into account and the dynamic loading behavior was analyzed in the field excavated soil with three different biochar amendment rates (i.e., 5%, 10%, and 15%). The novelty of this study is that the biochar was produced from waste peach endocarps and the cyclic load was imposed to the BAS in a self-designed apparatus (constant stiffness direct shear apparatus). The major reasoning for selecting the peach endocarp waste is due to the higher mechanical strength and high strain rate of the feedstock [34,35], which is expected to improve the mechanical strength of the soil. In the context of the apparatus, the designed setup maintains the constant stiffness loading so that the stress applied to the soil's contact surface is in the actual elastic area. Additionally, the larger size of the apparatus lessens the boundary effect hence the contact surface remains unchanged. Dynamic loading parameters such as shear modulus and damping ratio were determined and the results were compared between un-amended bare soil and BAS. Finally, the residual cyclic strength calculated were correlated with estimated void ratio values for better understanding the relation between BAS and corresponding dynamic load responses.

The overarching objective of this study is to present a preliminary understanding of the dynamic loading behavior of BAS. An in-house produced biochar from waste peach endocarps, were mixed with the soil at three different amendment in weight to weight proportions. The un-amended bare soil and BAS were tested in the designed constant stiffness direct shear apparatus to gauge the dynamic loading behavior.

2. Materials and Methodology

2.1. Soil Properties and New Biochar Production

The soil used in this study was collected from the coastal region of Qingdao city, Shandong province, China. It should be noted that the site was amenable to many offshore constructions and the offshore structures were susceptible to dynamic loads. The collected soil was characterized as per the American Standard of Testing and Materials (ASTM) provisions. The soil predominantly consists of clay (39%) trailed by silt (33%) and sand (28%) [36], thus the soil could be termed as silty clay as per the USCS classification [37]. The consistency limits of the soil were attained as a liquid limit value of 42.7% and plastic limit value of 27.5% [38]. The soil was also characterized for its compaction parameters using the modified standard proctor test [39]. The optimum moisture content and maximum dry density was found out to be 14.7% and 1.78 g/cm^3 respectively.

Peach endocarp wastes were collected from the local site and were pyrolyzed using the pyrolyzer. The whole pyrolysis process was executed in the absence of oxygen at a temperature of 400 °C for 3 h, which in general is termed as slow pyrolysis (Figure 1a) [40]. The produced biochar from the feedstock was crushed to powder and analyzed for its surface properties such as surface morphology and the functional groups. Figure 1b portrays the surface properties of the biochar, where the morphology and the functional groups were analyzed using Field Emission Scanning Electron Microscope (FE-SEM) and Fourier Transformation Infra-Red (FTIR) spectroscopy respectively. The figure shows that the Peach Endocarp (PE) biochar, being a plant-based feedstock possessed intrapores on the entirety of its surface. This high density of intrapores could be attributed to the thermal degradation of the simple biopolymers such as cellulose and hemicellulose, which degrades faster than the complex lignin [32,41,42]. The PE biochar was also enriched with the functional groups and had major hydrophilic functional group i.e., hydroxyl (OH^-), which was indicated by a prominent band around 3500 cm^{-1} wavelengths. The biochar also possessed other aromatic and aliphatic functional groups such as C-H, C-O, C-N, C=O, and so on, as represented in the figure. Addition to the surface parameters, PE biochar was examined for its elemental composition and molar ratios. The values obtained were presented in Table 1 with carbon, nitrogen, and hydrogen compositions.

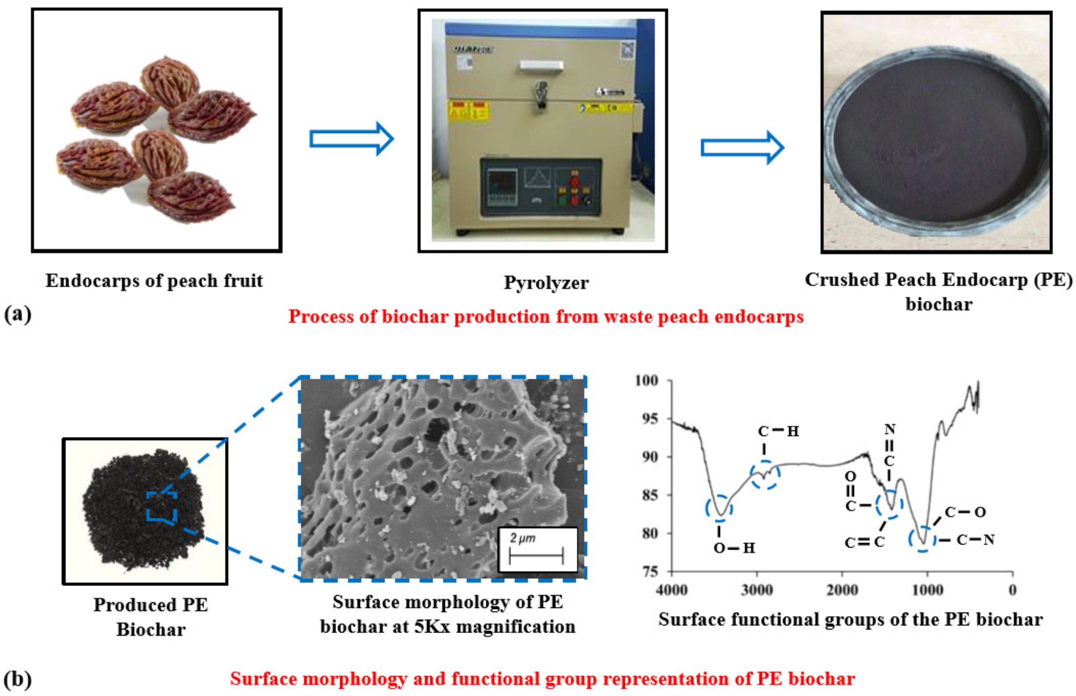

Figure 1. Illustration of Peach Endocarp (PE) biochar: (**a**) Production conditions and (**b**) surface properties.

Table 1. Properties of peach endocarps and biochar production specifications.

Feedstock	Peach Endocarps
Pyrolysis temperature (°C)	400
Pyrolysis process	Slow pyrolysis
Elemental composition	
Carbon (%)	54.6
Nitrogen (%)	2.9
Hydrogen (%)	3.6
Molar ratio	
C/N	18.8
H/C	0.07
Ash content (%)	21.6
Cation exchange capacity (cmol/kg^{-1})	13.72

2.2. Experimental Methodology

The dry soil was mixed with PE biochar at three different amendment rates (5%, 10%, and 15%) in weight to weight composition. The amended soils were characterized for its basic geotechnical properties and the respective results are listed in Table 2. Monotonic direct shear tests were conducted for the un-amended bare soil and the BAS at the compaction state of 0.9 MDD, where the test results could also be considered as a verification index for the designed constant stiffness direct shear apparatus. The monotonic direct shear test was carried out at a shear rate of 2 mm/min and normal load of 40 kN/mm^2. Furthermore, the bare soil and BAS were subjected to cyclic loading at the similar compaction state using the designed constant stiffness direct shear apparatus. The pictorial representation and the sample preparation for cyclic loading are picturized in Figure 2. The shear rate and normal load in the case of cyclic loading was kept at a rate of 5 mm/min and 40 kN/mm^2 respectively.

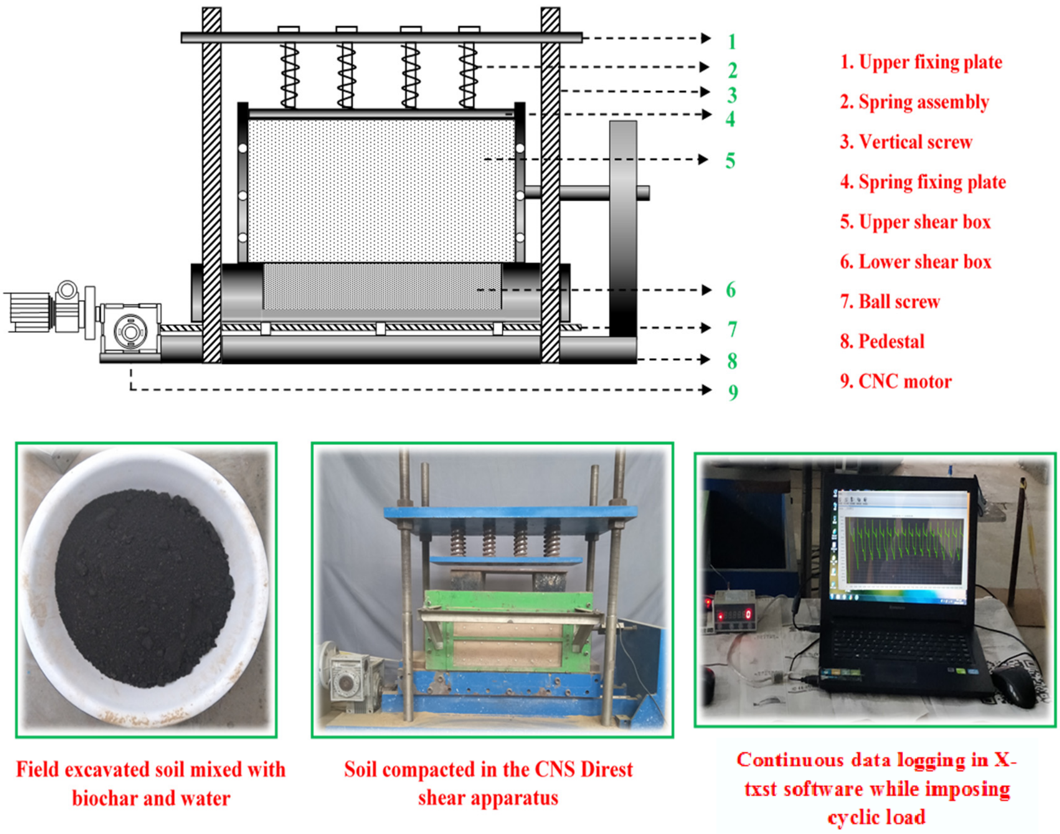

Figure 2. Schematic representation of the constant stiffness direct shear apparatus and test methodology for the cyclic shear test.

Table 2. Basic characterization of bare and Biochar Amended Soils (BAS).

Sample Designation	Consistency Limits [38]			Compaction Characteristics [39]		Specific Gravity [43]
	Liquid Limit (%)	Plastic Limit (%)	Plasticity Index	OMC (%)	MDD (g/cm^3)	
BS	42.7	27.5	15.2	14.7	1.78	2.53
PE	NA	NA	NA	NA	NA	0.74
BS+5% PE	46.4	29.3	17.1	15.2	1.71	2.29
BS+10% PE	49.8	32.1	17.7	16.7	1.64	2.18
BS+15% PE	53.3	34.9	18.4	18.3	1.59	2.10

2.3. Design and Development of Cyclic Loading System

The constant stiffness direct shear apparatus is a large, constant stiffness loading setup, located in Qingdao University of Technology, Shandong province, China. This apparatus was used to analyze the cyclic stress behavior of bare soil and BAS owing to its major instrumentation advantages. The apparatus could be classified into four major groups and the specifications are given below.

2.3.1. Constant Stiffness Loading System

The constant stiffness loading system is composed of vertical screw group, upper fixing plate, spring group, and spring fixing plate.

1. The vertical screw group consists of rounded thread rods, rigidly connecting the operating platform and the entire loading system at all the four corners. Each rod measures a diameter of 20 mm and a height of 800 mm;
2. The upper fixing plate is attached to the vertical screw group at all the four corners by means of screw and nut. The upper fixing plate has dimensions of 840 mm length and 540 mm breadth, while the thickness is maintained to 20 mm;
3. The upper fixing plate supports the spring group, where the springs enclosed the steel columns of 20 mm dia. The spring group consists of 8 standard springs which are divided into 2 equal pairs. The distance between two adjacent springs are maintained to 135 mm, both lengthwise and breadthwise;
4. The spring group firmly holds the spring fixing plate, where the dimensions of the plate is confirmed to a length of 700 mm and breadth of 300 mm. The thickness of the spring fixing plate is also maintained to 20 mm as in the case of upper fixing plate.

2.3.2. Interfacial Shear Simulation System

The interfacial shear simulation system consists of two parts, the upper and lower shear box.

1. The upper shear box is a closed box, having a dimension of 700 mm * 300 mm * 300 mm (length * breadth * height). The front face of the upper shear box is detachable by a steel plate of 20 mm thickness, and has a plexiglass window of size 500 mm * 210 mm;
2. The lower shear box is positioned just below the upper shear box and is a "U" groove made on the cut box. The lower shear box measures a dimension of 500 mm*300 mm*100 mm. The lower shear box is flexible to move back and forth during the shearing process.

2.3.3. Roller Bi-directional Transmission System

The roller bi-directional transmission system consists of platform, ball screw, CNC motor, and bi-directional control parts.

1. The platforms are made of steel and supports the entire instrument in both horizontal and vertical direction. The vertical platform's size is 1500 mm*500 mm*40 mm and the size of horizontal

platform is 500 mm*500 mm*40 mm in the order of length, breadth, and thickness respectively. Both the platforms are strengthened by connecting the ends using a trapezoidal rib plate;

2. The ball screw is composed of screw, nut ball, pre-stressing sheet, and dust proof device. The ball screw translates the rotational motion to linear motion with little friction and enables the shear box to move back and forth. The device uses Mishmi SFK_R00802 ball screw which facilitates the shear box to move 10 cm in a linear direction;
3. The CNC motor is operated by three major components i.e., frequency conversion motor, reducer, and frequency convertor device. The frequency conversion motor has the motor capacity of 2 kW with speed limit as 1500 rpm. The frequency of the motor is ranging between 5 Hz and 50 Hz. The shear rate of the reducer could be adjusted between 0.15 mm/min and 15 mm/min using the frequency convertor device. The frequency convertor is designed for self-adopting circuit, which senses the starting and termination of the shearing process automatically;
4. The bi-directional control parts have stroke switch and a scale. The stroke switch is directly connected to the frequency convertor and are provided at either sides of the shear box. This arrangement facilitates the shear box to reverse the direction after the specified displacement.

2.3.4. Data Acquisition System

The fundamental data collected for this experiment were normal stress and shear load at the shear plane, using a micro-earth pressure gauge and S-type load cell sensor respectively.

1. The shear load was determined using a "S" type load cell, which possess a spring element and 4 strain gauges in a wheat stone bridge formation. The deformation in the spring element is picked by the strain gauges and converts them into electric signal. The electric signals are further connected to DY220 high-precision weighing display controller, to obtain the shear load value;
2. The normal stress in the shear test was measured using two CL-YB-2 resistance strain type force sensors which are symmetrically arranged between the spring group and the loading stress. The data obtained from the sensor is logged to the computer using DH3816N static strain test system.

2.4. Determination of Dynamic Loading Parameters

Shear modulus and damping ratio are efficient and important parameters to estimate the dynamic loading responses of soil, as these parameters are directly related to the soil deformation properties [44,45]. These parameters can be determined from the hysteresis loop obtained from the cyclic shear test. Figure 3 represents a typical asymmetrical hysteresis loop, which portrays the conventional method of calculating shear modulus and damping ratio [46].

From the equations presented in the figure, shear modulus for each cycle can be calculated from the secant elastic modulus (E_{sec}) and Poisson's ratio (ϑ). The Poisson's ratio was considered to be 0.5 as per the recommendations in Rollins et al., 1998 [47]. Similarly the damping ratio for each cycle is computed using the area of the hysteresis loop and the area of the right triangle that forms under the maximum shear stress and maximum shear strain. Since the loop obtained is asymmetrical, the area of enclosed loop (A_L) is calculated as suggested by Kreyszig, 2010 [48].

$$A_L = \frac{1}{2}[(\in_1 *\sigma_2 - \in_2 *\sigma_1) + (\in_2 *\sigma_3 - \in_3 *\sigma_2) + \ldots + (\in_1 *\sigma_n - \in_n *\sigma_1) \quad (1)$$

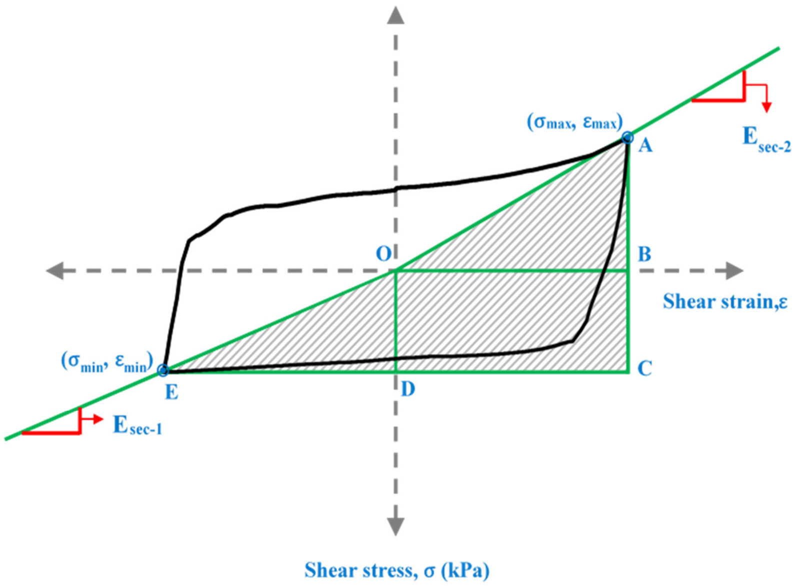

$$\textbf{\textit{Secant Elastic Modulus}}, E_{sec} = \frac{E_{sec-1} + E_{sec-2}}{2}$$

$$\textbf{\textit{Shear Modulus}} = \frac{E_{sec}}{2(1+\vartheta)}$$

$$\textbf{\textit{Damping ratio}} = \frac{1}{\pi} \frac{\textit{Area of the closed loop}}{\textit{Area } \Delta OAB + \textit{Area } \Delta ODE + \textit{Area OBCD}}$$

Figure 3. Schematic representation for shear modulus and damping ratio determination in an asymmetrical hysteresis loop.

2.5. Estimation of Void Ratio

The correlation between void ratio and cyclic stress behavior are similar to the influence of fines content. This unique relationship is clearly exemplified in several studies [49–51], affirming that decrease in void ratio increases the cyclic shear strength. In order to validate this statement, the void ratio was estimated from the following set of equations [52] and are associated with residual cyclic strength.

For partially saturated soil (three phase soil system):

$$\gamma_b = \frac{W_w + W_s}{V_v + V_s} \tag{2}$$

Since, weight=volume*density and $\gamma_s = G\gamma_w$

$$\gamma_b = \frac{V_w \cdot \gamma_w + V_s \cdot \gamma_s}{V_v + V_s} = \frac{V_w \cdot \gamma_w + V_s \cdot G \cdot \gamma_w}{V_v + V_s} = \frac{V_w + G \cdot V_s}{V_v + V_s} \cdot \gamma_w \tag{3}$$

Dividing the numerator and denominator by V_v, we get:

$$\gamma_b = \frac{\frac{V_w}{V_v} + \frac{G \cdot V_s}{V_v}}{\frac{V_v}{V_v} + \frac{V_s}{V_v}} \cdot \gamma_w \tag{4}$$

Given that, degree of saturation, $s = V_w / V_v$ and void ratio, $e = V_V / V_S$:

$$\gamma_b = \frac{s + \frac{G}{e}}{1 + \frac{1}{e}} \cdot \gamma_w = \frac{G + se}{1 + e} \cdot \gamma_w \tag{5}$$

Similarly $w = \frac{W_w}{W_s}$

Following the similar steps as in the case to derive Equation (1):

$$w = \frac{V_w \cdot \gamma_w}{V_s \cdot \gamma_s} = \frac{V_w \cdot \gamma_w}{V_s \cdot G \gamma_w} = \frac{\frac{V_w}{V_v}}{\frac{V_s \cdot G}{V_v}} = \frac{s}{\frac{G}{e}} \tag{6}$$

$se = wG$; $\gamma_b, \gamma_s, \gamma_w$ represents bulk density, density of solids, and density of water; W_w and W_s denotes weight of water and weight of solids; V_v, vs. and V_w denotes volume of voids, solids, and water individually; and G, e, s, and w represents specific gravity, void ratio, degree of saturation, and water content respectively.

From the known values of w and G, the multiple "$s \cdot e$" was found with respect to Equation (6). It is followed by the determination of void ratio using Equations (2)–(5) with known values of γ_b, γ_w, and G.

3. Results and Discussion

3.1. Stress-Strain Response on Monotonic Loading

The stress strain response provides the basic understanding of BAS on static loading, which is depicted in Figure 4. It can be observed from the graph that the peak shear stress in both BS+5% PE and BS+10% PE increases with respect to the bare soil. This is mainly attributed to the porous nature of the biochar particles. During static loading, the porous biochar particles is expected to undergo extensive particle rearrangement and facilitates an interlocking between the grains and biochar, restricting the free gain movement [53].

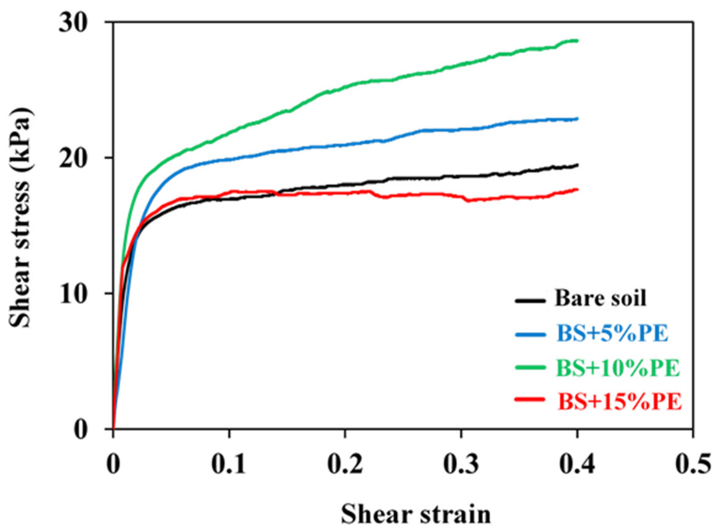

Figure 4. Stress-strain response under monotonic loading condition.

Despite the positive result at the first two cases, there is a contrasting trend in BS+15% PE, where the peak shear stress value is slightly decreased with respect to the bare soil. This peak value reduction could be ascribed to the formation of clay-carbon complexes at higher amendment rates [54]. The formation of clay-carbon complex was also observed in previous studies, where this complex reduces the interlocking mechanism between the biochar and soil grains [55]. In terms of numerical expressions, the peak shear stress value was increased with respect to the bare soil by 30% and 45% for BS+5% PE and BS+10% PE respectively. For BS+15% PE, the peak shear stress value was decreased to 8% with respect to the bare soil.

3.2. Dynamic Loading Characteristics

Figure 5 shows the stress-strain response of bare soil and BAS under cyclic loading. The stress-strain response for all the soil specimen follows an asymmetrical hysteresis loop trend and the hysteresis curves are smooth.

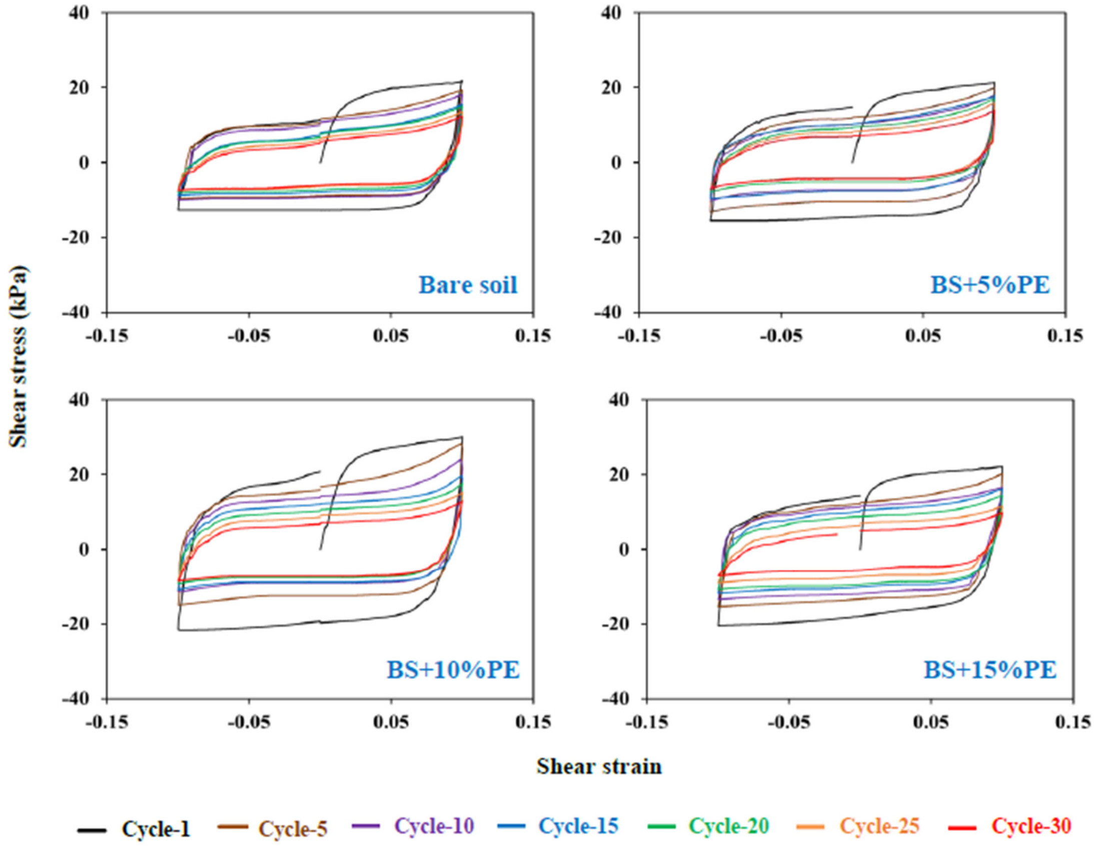

Figure 5. Asymmetrical hysterical loops of bare soil and BAS under cyclic loading test.

In order to compare the loading behavior between bare and BAS precisely, shear modulus and damping ratio values were computed and plotted against a number of cycles of loading (Figure 6). From the figure, it could be seen that there is a decrease in shear modulus of all soil types with an increase in the number of cycles. This reduction in shear modulus is evident due to an increase in the pore water pressure of compacted soil under cyclic loading [56]. Whilst, when comparing the results between the individual soil types, the shear modulus for all BAS increased with respect to the bare soil. This increment could be seen only in the first 15 cycles, later the modulus values were almost similar with the bare soil. On the other hand, there was not a significant change in the damping ratio, when the soil samples were compared.

Before devising a concluding remarks from the attained results, it is important to comprehend the influence factors of shear modulus and damping ratio. According to Hardin and Drnevich, 1972 [57], the major influence factors for these dynamic loading parameters were the number of cycles of loading, pore water pressure, and void ratio. Considering these factors, it is clear that the addition of biochar altered the void ratio and increased the soil dynamic modulus by maintaining the aspects of damping ratio.

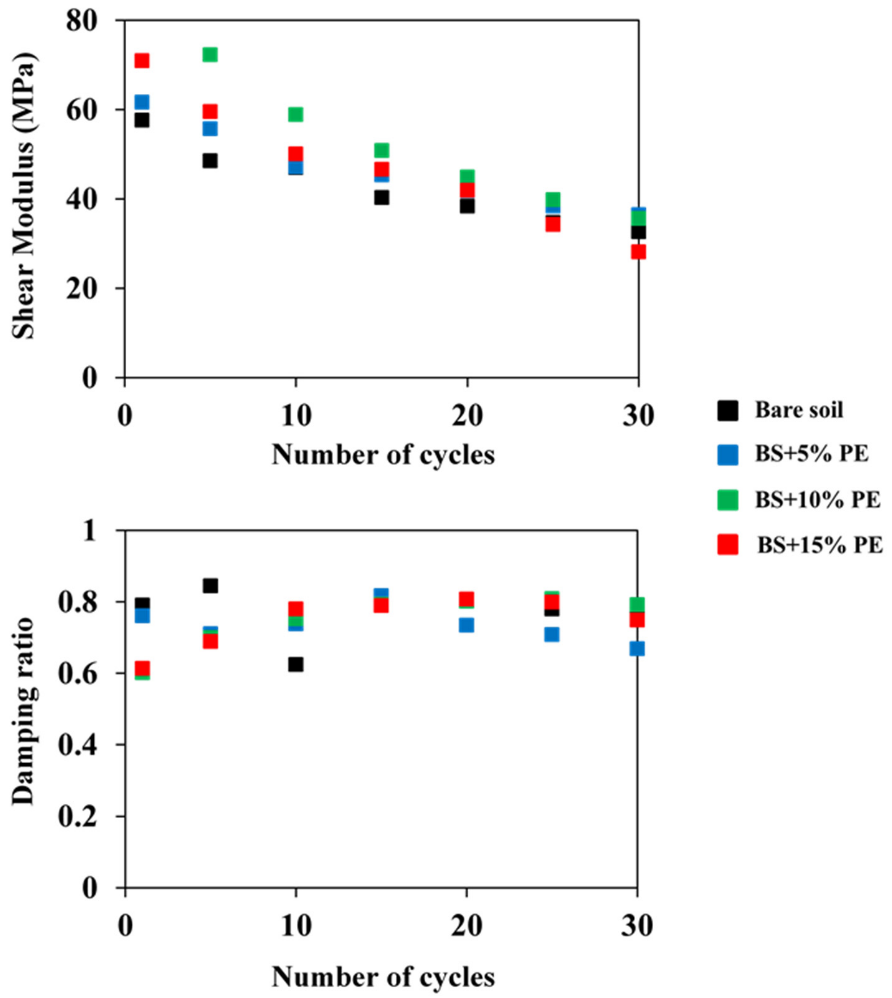

Figure 6. Comparison of shear modulus and damping ratio results between bare soil and BAS.

3.3. Interrelation between Residual Cyclic Strength and Void Ratio

The residual cyclic strength measured at each cycle for bare and BAS is presented in Figure 7a and the estimated void ratio for the compacted soil specimens are graphically represented in Figure 7b.

From the residual cyclic strength, it could be seen that the strength increased in BS+5% PE and BS+10% PE was mainly observed in the first 15 cycles, then the residual cyclic strength levels off and resembled bare soil. Alternatively, the void ratio values decreased with an increase in amendment rates. This clearly indicates that the decrease in void ratio increased the cyclic residual strength by means of better interlocking between the biochar and soil grains in the first 15 cycles. Thereafter, the residual cyclic strength attenuated and yielded a similar strength to the bare soil. This is logically assumed that after certain number of cycles, capillary pressure inside the pores of the biochar builds up pore water pressure and attenuates the residual cyclic strength. This phenomenon is supported by the fact that capillary pressure is indirectly proportional to the diameter of the pores [58]. Nonetheless, it is also clear that the residual cyclic strength of BS+15% PE decreased with respect to the bare soil. This is again attributed to the clay-carbon complex between biochar and soil grains, which disrupts the interlocking mechanism, neglecting the void ratio decrement [54].

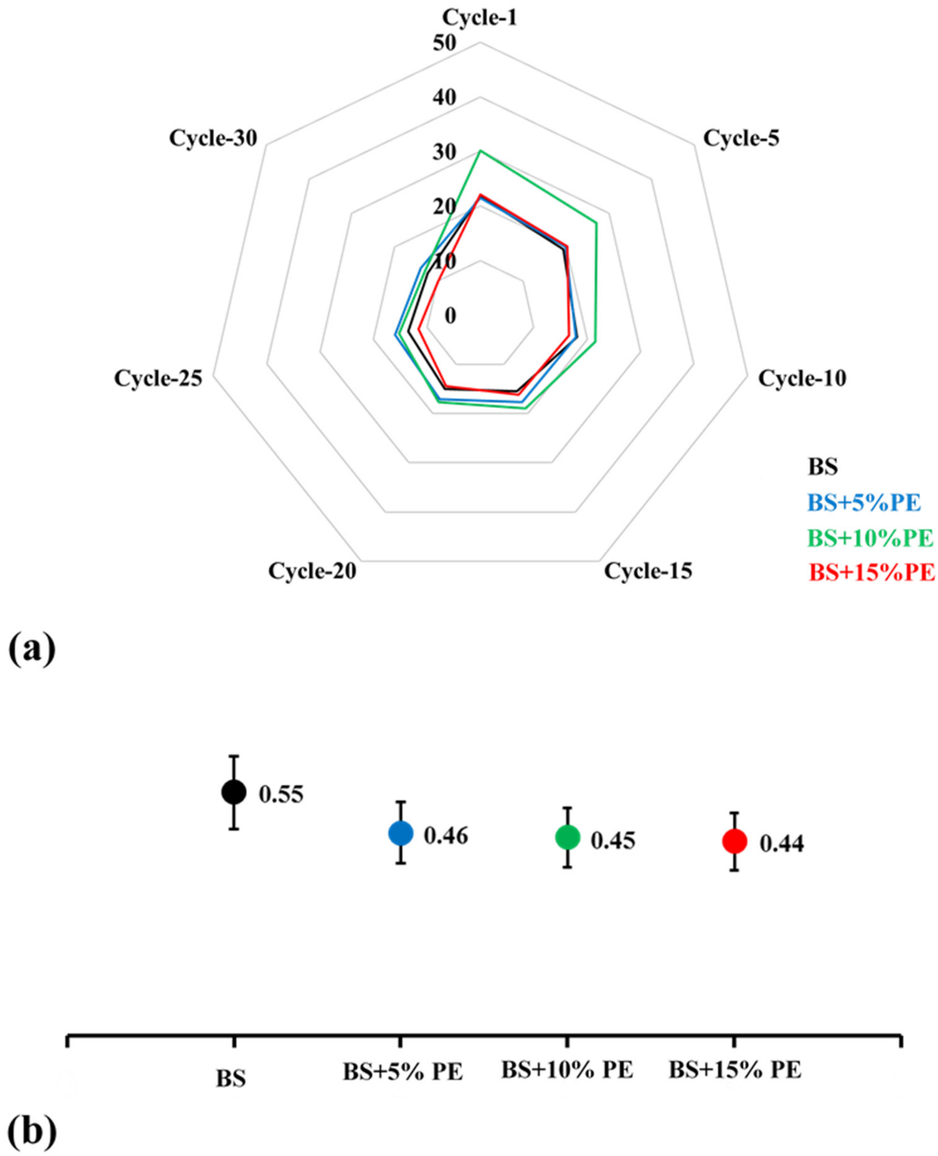

Figure 7. (**a**) Residual cyclic strength of bare soil and BAS at each cycle and (**b**) estimated void ratio of compacted soil specimen.

4. Conclusions

It is important to emphasize that the results shown is limited only to the biochar produced from peach endocarp wastes. The results showed that the addition of biochar decreased the void ratio, which facilitated the BAS to produce an interlocking mechanism between the biochar and soil and increased the shear modulus and residual cyclic strength. However, this mechanism was effective only for the first 15 cycles and then the shear modulus and residual cyclic strength attenuated due to an increase in pore water pressure, caused by capillary pressure in the biochar pores. On the contrary, beyond certain amendment rate, BAS forms a clay-carbon complex, which disrupted the interlocking mechanism. Therefore the study concluded that biochar could be considered as a potential material for landfill liners and pre-soil amendment in offshore constructions where the dynamic loads are prone, instead of using environmentally hazardous additives.

Author Contributions: J.L. and A.G. conceived the idea; X.L., A.S. and K.D.D. designed and conducted the experiment; J.L., S.P.G. and A.G. analyzed the results; S.P.G., and A.G. prepared the manuscript; J.L., X.L. and H.F. All authors have read and agreed to the published version of the manuscript.

Funding: This research was funded by National Natural Science Foundation of China (41772318), Qingdao Fundamental Research Project (16-5-1-34-jch) and National Natural Science Foundation Youth Project (Project number 41907252). And the APC was funded by Shandong Key Research and Development Plan (2017GSF20107) and Open Fund of State Key Laboratory of Coastal and Offshore Engineering (LP1712).

Conflicts of Interest: The authors declare no competing conflict of interest.

References

1. Budarin, V.; Clark, J.; Lanigan, B.A.; Shuttleworth, P.S.; MacQuarrie, D. Microwave assisted decomposition of cellulose: A new thermochemical route for biomass exploitation. *Bioresour. Technol.* **2010**, *101*, 3776–3779. [CrossRef]
2. Kabir, R.; Kumar, A. Comparison of the energy and environmental performances of nine biomass/coal co-firing pathways. *Bioresour. Technol.* **2012**, *124*, 394–405. [CrossRef] [PubMed]
3. Chowdhury, R.; Viamajala, S.; Gerlach, R. Reduction of environmental and energy footprint of microalgal biodiesel production through material and energy integration. *Bioresour. Technol.* **2012**, *108*, 102–111. [CrossRef] [PubMed]
4. Carlile, W.; Raviv, M.; Prasad, M. Organic Soilless Media Components. *Soilless Culture* **2019**, 303–378.
5. McKendry, P. Energy production from biomass (Part 2): Conversion technologies. *Bioresour. Technol.* **2002**, *83*, 47–54. [CrossRef]
6. Smith, P. Soil carbon sequestration and biochar as negative emission technologies. *Glob. Chang. Boil.* **2016**, *22*, 1315–1324. [CrossRef]
7. Moreira, M.T.; Noya, I.; Feijoo, G. The prospective use of biochar as adsorption matrix–A review from a lifecycle perspective. *Bioresour. Technol.* **2017**, *246*, 135–141. [CrossRef]
8. Lee, J.W.; Hawkins, B.; Day, D.M.; Reicosky, D.C. Sustainability: The capacity of smokeless biomass pyrolysis for energy production, global carbon capture and sequestration. *Energy Environ. Sci.* **2010**, *3*, 1695. [CrossRef]
9. De Oliveira, F.R.; Patel, A.K.; Jaisi, D.P.; Adhikari, S.; Lu, H.; Khanal, S.K. Environmental application of biochar: Current status and perspectives. *Bioresour. Technol.* **2017**, *246*, 110–122. [CrossRef]
10. Bordoloi, S.; Garg, A.; Sreedeep, S.; Peng, L.; Mei, G. Investigation of cracking and water availability of soil-biochar composite synthesized from invasive weed water hyacinth. *Bioresour. Technol.* **2018**, *263*, 665–677. [CrossRef]
11. Garg, A.; Huang, H.; Kushvaha, V.; Madhushri, P.; Kamchoom, V.; Wani, I.; Koshy, N.; Zhu, H.-H. Mechanism of biochar soil pore–gas–water interaction: Gas properties of biochar-amended sandy soil at different degrees of compaction using KNN modeling. *Acta Geophys.* **2019**, *68*, 207–217. [CrossRef]
12. Kumar, H.; Cai, W.; Lai, J.; Chen, P.; Ganesan, S.P.; Bordoloi, S.; Liu, X.; Wen, Y.; Garg, A.; Mei, G. Influence of in-house produced biochars on cracks and retained water during drying-wetting cycles: Comparison between conventional plant, animal, and nano-biochars. *J. Soils Sediments* **2020**, *20*, 1983–1996. [CrossRef]
13. Yaghoubi, P.; Reddy, K.R. Characteristics of biochar amended soil cover for landfill gas mitigation. In Proceedings of the Pan-Am CGS Geotechnical Conference, Toronto, ON, Canada, 2–6 October 2011.
14. Chen, X.-W.; Wong, J.T.F.; Ng, C.W.W.; Wong, M. Feasibility of biochar application on a landfill final cover—a review on balancing ecology and shallow slope stability. *Environ. Sci. Pollut. Res.* **2015**, *23*, 7111–7125. [CrossRef] [PubMed]
15. Das, O.; Sarmah, A.K. The love–hate relationship of pyrolysis biochar and water: A perspective. *Sci. Total Environ.* **2015**, *512*, 682–685. [CrossRef]
16. Wong, J.T.F.; Chen, Z.; Chen, X.; Ng, C.W.W.; Wong, M. Soil-water retention behavior of compacted biochar-amended clay: A novel landfill final cover material. *J. Soils Sediments* **2016**, *17*, 590–598. [CrossRef]
17. Basso, A.S.; Miguez, F.; Laird, D.A.; Horton, R.; Westgate, M. Assessing potential of biochar for increasing water-holding capacity of sandy soils. *GCB Bioenergy* **2012**, *5*, 132–143. [CrossRef]
18. Grunwald, D.; Kaiser, M.; Ludwig, B. Effect of biochar and organic fertilizers on C mineralization and macro-aggregate dynamics under different incubation temperatures. *Soil Tillage Res.* **2016**, *164*, 11–17. [CrossRef]
19. Kookana, R.S.; Sarmah, A.K.; Van Zwieten, L.; Krull, E.; Singh, B. Biochar Application to Soil. *Adv. Agron.* **2011**, *112*, 103–143.

20. Chan, K.Y.; Xu, Z. Biochar: Nutrient properties and their enhancement. In *Biochar for Environmental Management: Science and Technology*; Lehmann, J., Joseph, S., Eds.; Routledge: London, UK, 2009; pp. 67–84.
21. Laird, D.A.; Fleming, P.; Davis, D.D.; Horton, R.; Wang, B.; Karlen, D.L. Impact of biochar amendments on the quality of a typical Midwestern agricultural soil. *Geoderma* **2010**, *158*, 443–449. [CrossRef]
22. Tripathi, M.; Sahu, J.N.; Ganesan, P.B. Effect of process parameters on production of biochar from biomass waste through pyrolysis: A review. *Renew. Sustain. Energy Rev.* **2016**, *55*, 467–481. [CrossRef]
23. Reddy, K.R.; Yaghoubi, P.; Yukselen-Aksoy, Y. Effects of biochar amendment on geotechnical properties of landfill cover soil. *Waste Manag. Res.* **2015**, *33*, 524–532. [CrossRef] [PubMed]
24. Wong, J.T.F.; Chen, Z.; Wong, A.Y.Y.; Ng, C.W.W.; Wong, M. Effects of biochar on hydraulic conductivity of compacted kaolin clay. *Environ. Pollut.* **2018**, *234*, 468–472. [CrossRef] [PubMed]
25. Kumar, H.; Ganesan, S.P.; Bordoloi, S.; Sreedeep, S.; Lin, P.; Mei, G.; Garg, A.; Sarmah, A.K. Erodibility assessment of compacted biochar amended soil for geo-environmental applications. *Sci. Total Environ.* **2019**, *672*, 698–707. [CrossRef] [PubMed]
26. Liu, Z.; Dugan, B.; Masiello, C.A.; Barnes, R.T.; Gallagher, M.; Gonnermann, H. Impacts of biochar concentration and particle size on hydraulic conductivity and DOC leaching of biochar–sand mixtures. *J. Hydrol.* **2016**, *533*, 461–472. [CrossRef]
27. Rizwan, M.; Ali, S.; Qayyum, M.F.; Ibrahim, M.; Zia-Ur-Rehman, M.; Abbas, T.; Ok, Y.S. Mechanisms of biochar-mediated alleviation of toxicity of trace elements in plants: A critical review. *Environ. Sci. Pollut. Res.* **2015**, *23*, 2230–2248. [CrossRef]
28. Christakos, G. Soil behavior under dynamic loading conditions: Experimental procedures and statistical trends. *Environ. Res. Risk Assess.* **2003**, *17*, 175–190. [CrossRef]
29. Liu, J.; Guo, Z.; Zhu, N.; Zhao, H.; Garg, A.; Xu, L.; Liu, T.; Fu, C. Dynamic Response of Offshore Open-Ended Pile under Lateral Cyclic Loadings. *J. Mar. Sci. Eng.* **2019**, *7*, 128. [CrossRef]
30. Matasovic, N.; Kavazanjian, E. Seismic response of composite landfill liner. *J. Geotech. Geoenviron.* **2006**, *132*, 448–455. [CrossRef]
31. Patel, A. *Geotechnical Investigations and Improvement of Ground Conditions*, 1st ed.; Woodhead, Cambridge Press: Cambridge, UK, 2019.
32. Pardo, G.; Orense, R.; Sarmah, A. Cyclic strength of sand mixed with biochar: Some preliminary results. *Soils Found.* **2018**, *58*, 241–247. [CrossRef]
33. Pardo, G.S.; Sarmah, A.K.; Orense, R. Mechanism of improvement of biochar on shear strength and liquefaction resistance of sand. *Géotechnique* **2019**, *69*, 471–480. [CrossRef]
34. Nakano, M.; Nakamura, M. Cracking and Mechanical Properties of the Stone in peach cultivars after severe thinning. *Acta Hortic.* **2002**, *592*, 531–536. [CrossRef]
35. Buchar, J.; Nedomova, S.; Severa, L. High strain rate behavior of peaches. In Proceedings of the 2008 SEM XI International Congress and Exposition on Experimental and Applied Mechanics, Orlando, FL, USA, 2–5 June 2008; pp. 163–170.
36. ASTM D422-63. *Standard Test Method for Particle Size Analysis of Soils; Annual Book of ASTM Standards*; ASTM International: West Conshohocken, PA, USA, 2007.
37. ASTM D2487. *Standard Practice for Classification of Soils for Engineering Purposes (Unified Soil Classification System), Annual Book of ASTM Standards*; ASTM International: West Conshohocken, PA, USA, 2017.
38. ASTM D4318. *Standard Test Methods for Liquid Limit, Plastic Limit and Plasticity Index of Soils, Annual Book of ASTM Standards*; ASTM International: West Conshohocken, PA, USA, 2010.
39. ASTM D1557. *Standard Test Methods for Laboratory Compaction Characteristics of Soil Using Modified Effort (56,000 ft-lbf/ft3 (2700 kN-m/m3)), Annual Book of ASTM Standards*; ASTM International: West Conshohocken, PA, USA, 2015.
40. Huang, Z.; Li, N.; Zhou, Q.; Wang, D.; Yin, H. A comparative study of the pyrolysis and combustion characteristics of sodium-rich Zhundong coal in slow and rapid processes. *Energy Sci. Eng.* **2018**, *7*, 98–107. [CrossRef]
41. Lehmann, J.; Joseph, S. (Eds.) *Biochar for Environmental Management: Science, Technology and Implementation*; Routledge: London, UK, 2015.
42. Bordoloi, S.; Gopal, P.; Boddu, R.; Wang, Q.; Cheng, Y.-F.; Garg, A.S.S.; Qinhua, W.; Feng, Y.-C.; Sreedeep, S. Soil-biochar-water interactions: Role of biochar from Eichhornia crassipes in influencing crack propagation and suction in unsaturated soils. *J. Clean. Prod.* **2019**, *210*, 847–859. [CrossRef]

43. ASTM D845. *Standard Test Methods for Specific Gravity of Soil Solids by Water Pycnometer*; ASTM International: West Conshohocken, PA, USA, 2014.
44. Mojezi, M.; Biglari, M.; Jafari, M.K.; Ashayeri, I. Determination of shear modulus and damping ratio of normally consolidated unsaturated kaolin. *Int. J. Geotech. Eng.* **2018**, *14*, 264–285. [CrossRef]
45. Kucharczyk, K.; Głuchowski, A.; Miturski, M.; Sas, W. Influence of Load Frequency on Cohesive Soil Respond. *Geosciences* **2018**, *8*, 468. [CrossRef]
46. ASTM D3999. *Standard Test Methods for the Determination of the Modulus and Damping Properties of Soils Using the Cyclic Triaxial Apparatus*; ASTM International: West Conshohocken, PA, USA, 2011.
47. Rollins, K.M.; Evans, M.D.; Diehl, N.B.; Iii, W.D.D. Shear Modulus and Damping Relationships for Gravels. *J. Geotech. Geoenviron. Eng.* **1998**, *124*, 396–405. [CrossRef]
48. Kreyszig, E. *Advanced Engineering Mathematics*; John Wiley & Sons: Hoboken, NJ, USA, 2010.
49. Belkhatir, M.; Schanz, T.; Arab, A. Effect of fines content and void ratio on the saturated hydraulic conductivity and undrained shear strength of sand–silt mixtures. *Environ. Earth Sci.* **2013**, *70*, 2469–2479. [CrossRef]
50. Kim, U.; Kim, D.; Zhuang, L. Influence of fines content on the undrained cyclic shear strength of sand–clay mixtures. *Soil Dyn. Earthq. Eng.* **2016**, *83*, 124–134. [CrossRef]
51. Porcino, D.D.; Diano, V. The influence of non-plastic fines on pore water pressure generation and undrained shear strength of sand-silt mixtures. *Soil Dyn. Earthq. Eng.* **2017**, *101*, 311–321. [CrossRef]
52. Arora, K.R. *Soil Mechanics and Foundation Engineering*, 7th ed.; Standard Publications: Delhi, India, 2008.
53. Sadasivam, B.Y.; Reddy, K.R. Engineering properties of waste wood-derived biochars and biochar-amended soils. *Int. J. Geotech. Eng.* **2015**, *9*, 521–535. [CrossRef]
54. Zong, Y.; Chen, D.; Lu, S. Impact of biochars on swell-shrinkage behavior, mechanical strength, and surface cracking of clayey soil. *J. Plant Nutr. Soil Sci.* **2014**, *177*, 920–926. [CrossRef]
55. Sadasivam, B.Y.; Reddy, K.R. Shear strength of waste–wood biochar and biochar–amended soil used for sustainable landfill cover systems. In *From Fundamentals to Applications in Geotechnics*; Manzanal, D., Sfriso, A.O., Eds.; IOS Press: Amsterdam, The Netherlands, 2015; pp. 745–752.
56. Brandon, T.L.; Rose, A.T.; Duncan, J.M. Drained and Undrained Strength Interpretation for Low-Plasticity Silts. *J. Geotech. Geoenviron. Eng.* **2006**, *132*, 250–257. [CrossRef]
57. Hardin, B.O.; Drnevich, V.P. Shear modulus and damping in soils: Measurement and parameter effects. *J. Soil. Mech. Found. Div.* **1972**, *98*, 603–624.
58. Kralchevsky, P.A.; Danov, K.D. Interactions between Particles at a Fluid Interface. In *Nanoscience: Colloidal and Interfacial Aspects*; Starov, V.M., Ed.; CRC Press: Boca Raton, FL, USA, 2010; pp. 397–435.